Published in final edited form as:
Cell. 2014 April 24; 157(3): 651–663. doi:10.1016/j.cell.2014.03.049.

CLP1 Founder Mutation Links tRNA Splicing and Maturation to Cerebellar Development and Neurodegeneration

Ashleigh E. Schaffer[1], **Veerle R.C. Eggens**[2], **Ahmet Okay Caglayan**[3], **Miriam S. Reuter**[4], **Eric Scott**[1], **Nicole G. Coufal**[1], **Jennifer L. Silhavy**[1], **Yuanchao Xue**[5], **Hulya Kayserili**[6], **Katsuhito Yasuno**[3], **Rasim Ozgur Rosti**[1], **Mostafa Abdellateef**[1], **Caner Caglar**[3], **Paul R. Kasher**[2], **J. Leonie Cazemier**[2], **Marian A. Weterman**[2], **Vincent Cantagrel**[1,7], **Na Cai**[1], **Christiane Zweier**[4], **Umut Altunoglu**[6], **N. Bilge Satkin**[6], **Fesih Aktar**[8], **Beyhan Tuysuz**[9], **Cengiz Yalcinkaya**[10], **Huseyin Caksen**[11], **Kaya Bilguvar**[3], **Xiang-Dong Fu**[5], **Christopher Trotta**[12], **Stacey Gabriel**[13], **André Reis**[4], **Murat Gunel**[3,14], **Frank Baas**[2,14], and **Joseph G. Gleeson**[1,14]

[1]Neurogenetics Laboratory, Howard Hughes Medical Institute, Department of Neurosciences, University of California, San Diego, CA 92093, USA [2]Department of Genome Analysis, Academic Medical Center, Meibergdreef 9, 1105AZ Amsterdam, The Netherlands [3]Yale Program on Neurogenetics, Departments of Neurosurgery, Neurobiology and Genetics, Yale University, School of Medicine, New Haven, Connecticut 06510, USA. [4]Institute of Human Genetics, Universität Erlangen-Nürnberg, Schwabachanlage 10, Erlangen 91054, Germany [5]Cellular Molecular Medicine, University of California, San Diego, CA 92093, USA. [6]Medical Genetics Department, Istanbul Medical Faculty, Istanbul University, Millet Caddesi, 34093 Fatih/Istanbul, Turkey [7]Institut IMAGINE, INSERM U1163, Faculté Paris-Descartes, Paris, France [8]Department of Pediatrics, Diyarbakir State Hospital, 21100 Diyarbakir, Turkey [9]Department of Pediatric Genetics, Cerrahpaşa Medical School, Istanbul University, 34098 Istanbul, Turkey [10]Department of Neurology, Division of Child Neurology, Cerrahpaşa Medical School, Istanbul University, 34098 Istanbul, Turkey [11]Department of Pediatrics, Meram Medical School, Necmettin Erbakan

Correspondence to: J.G.G. jogleeson@ucsd.edu.
[14]Co-Senior Authors

AUTHOR CONTRIBUTIONS J.L.S, A.O.C. and M.S.R. independently identified *CLP1* mutation in patient cohorts. A.E.S performed all experiments except those involving zebrafish and tandem affinity purification, performed by V.R.C.E and C.T, respectively. A.E.S, N.G.C. and Y.X performed iNeuron experiments. F.B. and J.G.G. coordinated the fish study. A.E.S and J.G.G. wrote the manuscript, edited by all co-authors.

Accession Numbers. Exome sequencing data have been deposited to dbGAP phs000288.v1.p1. Refseq ID human *CLP1*: Gene: NM_006831.2; Protein: NP_006822.1, Yeast *clp1* Q08685, Zebrafish *clp1* (*LOC565621*): XM_688892.4, Zebrafish *hspc117* (rtcb): NM_213103.1.

Supplemental Information is linked to the manuscript.

WEB RESOURCES
The URLs for data presented herein are as follows:
Online Mendelian Inheritance in Man (OMIM), http://www.omim.org
SeattleSeq Annotation, *http://gvs.gs.washington.edu*
UCSC Genome browser, *http://www.genome.ucsc.edu*
Universal Protein Resource, *http://uniprot.org*
Human Brain Transcriptome database, http://www.humanbraintranscriptome.org
Exome data deposited at dbGaP http://www.ncbi.nlm.nih.gov/gap phs000288.v1.p1

COMPETING FINANCIAL INTERESTS
The authors declare no competing financial interests.

University, 42080 Konya, Turkey [12]PTC Therapeutics, South Plainfield, NJ 07080, USA [13]Broad Institute of Harvard and Massachusetts Institute of Technology, Cambridge, MA 02142, USA

SUMMARY

Neurodegenerative diseases can occur so early as to affect neurodevelopment. From a cohort of over 2000 consanguineous families with childhood neurological disease, we identified a founder mutation in four independent pedigrees in *cleavage and polyadenylation factor I subunit* (*CLP1*). CLP1 is a multifunctional kinase implicated in tRNA, mRNA and siRNA maturation. Kinase activity of the CLP1 mutant protein was defective, and the tRNA endonuclease complex (TSEN) was destabilized, resulting in impaired pre-tRNA cleavage. Germline *clp1* null zebrafish showed cerebellar neurodegeneration that was rescued by wild type but not mutant human *CLP1* expression. Patient-derived induced neurons displayed both depletion of mature tRNAs and accumulation of unspliced pre-tRNAs. Transfection of partially processed tRNA fragments into patient cells exacerbated an oxidative stress-induced reduction in cell survival. Our data links tRNA maturation to neuronal development and neurodegeneration through defective CLP1 function in humans.

Keywords

CLP1; tRNA splicing endonuclease complex; TSEN; ataxia; neurodegeneration

INTRODUCTION

Transfer RNAs (tRNAs) are abundantly expressed RNA molecules required to bring amino acids to the translating ribosome for protein synthesis. Of the 506 known human tRNAs, 32 are encoded as pre-tRNAs, containing introns that are spliced during maturation (Lowe and Eddy, 1997; Phizicky and Hopper, 2010). The nuclear-localized tRNA splicing endonuclease (TSEN) complex recognizes the secondary structure of pre-tRNA molecules and cleaves at the exon-intron boundaries to yield a 2',3'-cyclic phosphate (i.e. phosphodiester) and 5'-OH terminal at the splice site (Peebles et al., 1983). Although still the subject of some debate, there are at least two proposed mechanisms of re-ligating these "half" tRNAs in mammals (i.e. the 5'-and 3'-exons remaining after excision of the single intron). In the first, HSPC117 directly mediates the ligation of these ends, utilizing the phosphate from the phosphodiester bond in the linkage, and is inhibited by the presence of a 5'-phosphorylation (Popow et al., 2011). In the second, 5'-phosphorylation by CLP1, a component of the TSEN complex in mammals, is required (Paushkin et al., 2004; Weitzer and Martinez, 2007; Zillmann et al., 1991), but the ligase that follows has not yet been discovered. Utilization of both pathways in human cells is documented, but their relative importance and functional redundancy in development and homeostasis remains unclear.

Pontocerebellar hypoplasia represents a group of inherited progressive neurodegenerative disorders with prenatal onset, thus intersecting development with degeneration. All subtypes share common structural defects of the pons and cerebellum, evident upon brain imaging. Targeted therapy is non-existent, and most patients die during infancy (Namavar et al.,

2011b). Mutations in any of three subunits of the TSEN complex, in the mitochondrial arginyl-tRNA synthetase gene, the RNA exosome component EXOSC3, and the vaccine related kinase are found in some cases (Budde et al., 2008; Edvardson et al., 2007; Renbaum et al., 2009; Wan et al., 2012). We recently implicated AMPD2 in PCH, causing a defect in protein translation due to guanosine triphosphate depletion (Akizu et al., 2013). The data implicate RNA maturation and protein synthesis defects in PCH, but also suggest further causes are yet to be identified.

Here we demonstrate a requirement for *CLP1* in human brain development. We identify four independent families carrying a founder p.R140H which impairs affinity for the TSEN complex, kinase activity in a recombinant assay, as well as function *in vivo*. Consistent with its role tRNA splicing, we find depleted mature tRNAs and excessive pre-tRNAs accumulating in patient-derived induced neurons (iNeurons). We demonstrate sensitivity of patient cells to oxidative-stress induced death exacerbated by the addition of unphosphorylated 3'-tRNA-exon halves and partially corrected with 5'-phospho- 3'-tRNA exon addition. In sum, we uncover an evolutionarily conserved requirement for CLP1 during vertebrate neurogenesis, and show CLP1 is necessary for tRNA maturation, the loss of which leads to stress-induced cell death.

RESULTS

Patients harboring *CLP1* mutation have progressive brain atrophy

We collaboratively recruited over 2000 families, most with documented parental consanguinity, presenting a child with neurological disease. We performed exome sequencing on at least one affected member per family, then analyzed each for potentially deleterious homozygous mutations. GATK (DePristo et al., 2011) was used for variant identification and intersected with identity-by-descent blocks from HomozygosityMapper (Seelow et al., 2009). Rare potentially deleterious variants were prioritized against our cumulative in-house 4000 patient exome database and across publically available exome datasets, cumulatively numbering over 10,000 individuals. From this analysis, four independent consanguineous Turkish families with a neurodevelopmental/neurodegenerative disorder emerged (Figure 1A), all displaying an identical homozygous Chr. 11:57427367G>A (hg19) single nucleotide transition in the *CLP1* gene, resulting in a p.ARG140HIS (p.R140H) amino acid substitution mutation.

Following the identification of the mutation, it became clear that the patients shared many clinical features, but it would have been difficult to separate them clinically from the rest of the cohort. After an unremarkable perinatal history, onset of slow, progressive, neurodegenerative features and/or static encephalopathy ensued by 6 months of age. Clinical features included failure to develop gross or fine motor skills, absent or delayed speech, progressive spasticity and spontaneous epileptic seizures (Table 1 and Table S1). Brain MRI demonstrated mild atrophy of the cerebellum, pons and corpus callosum (Figure 1B), together with progressive microcephaly. Electromyography, while initially normal at a young age, demonstrated age-dependent muscle fibrillations and high amplitude motor unit potentials in one patient, indicating progressive spinal motor neuron loss. Extensive testing

for known metabolic or degenerative diseases was negative, suggesting a here-to-fore unknown condition.

The mutant allele was observed heterozygous twice in unrelated unaffecteds in our in-house exome database of collectively over 2000 independent exomes (including about 1000 Turkish individuals), and not reported in any public database, suggesting a carrier frequency of 1:1000. In all families, we confirmed that the mutation occurred within a homozygous haplotype block (Figure S1A), suggesting a founder mutation. The mutated amino acid residue was highly conserved in all multicellular organisms (Figure 1C), and predicted to be damaging (Adzhubei et al., 2010). No other potentially deleterious rare homozygous *CLP1* variants were present in the database. Comparison of exome allele calls between families suggested a minimal shared haplotype between chr11:57317640-57461472, or 143,832 bp (Figure S1B), dated to a common ancestor approximately 16.2 generations in the past (+/− 8.7 generations, see methods), during the height of the Ottoman expansion.

Direct Sanger sequence analysis of all available family members, including deceased member 1810-VI-2 (from dried umbilical cord) demonstrated segregation according to a strict recessive mode of inheritance (Figure S1C), consistent with pathogenesis. Obligate carriers were entirely normal. We further found no other *CLP1* mutations in any other patient in our collective cohorts with overlapping clinical features, nor any from an additional directly sequenced cohort of 100 cases with familial motor neuron disease.

$CLP1^{R140H}$ is functionally compromised

To determine if the mutation was predicted to disrupt protein function, we modeled human CLP1 using the structure of the partially crystallized yeast nucleotide-bound Clp1 (Noble et al., 2007). In yeast, the p.140ARG is substituted for a LYS at the cognate position, which is also a polar basic residue (p.149LYS). Structure shows that the yeast p.149LYS is involved in the formation of an inferred hydrogen bond with the highly conserved p.59GLU residue (Figure 2A). This polar contact is predicted to be maintained in human, but disrupted in the presence of the mutant p.140HIS residue, suggesting an alteration in protein structure or function. We found comparable CLP1 protein levels among all genotypes in primary fibroblast lysates derived from skin biopsy (Figure 2B), suggesting protein stability was unaltered in the presence of the mutation.

The p.R140H mutation occurred right after the ATP-binding P-loop (i.e. Walker A motif), conserved in all kinases. To determine if the mutation alters CLP1 kinase activity we tested recombinant wild type (wt) and mutant GST-tagged human CLP1 protein against a poly(A) RNA oligonucleotide natural kinase substrate in an established assay (Ramirez et al., 2008). Recombinant mutant p.R140H CLP1 was stable to purification (Figure S2A) but displayed defective kinase activity, reduced by more than half of wt levels (Figure 2C). We conclude that CLP1 kinase activity was functionally impaired as a result of the p.R140H mutation.

We found that *CLP1*, each of the known *TSENs*, and *HSPC117* were expressed ubiquitously in 14 human tissues and ages tested (Figure S2B), suggesting a conserved function. Therefore, to understand the selective cellular vulnerability, we generated induced neurons (iNeurons) from affected and unaffected fibroblasts, using recently published methods (Xue

et al., 2013), yielding approximately 80% neural cells in culture (Figure S2C-E). Both patient fibroblasts and iNeurons showed reduced nuclear localized CLP1, supported by nuclear/cytoplasmic fibroblast cell fractionation (Figure 2D-E). We conclude that the p.R140H mutation results in both failed nuclear localization and impaired kinase activity, as a mechanism of impaired function.

Mutant zebrafish phenocopy *CLP1*^{R140H} mutant patients

Recent work in mice suggests an essential function for *Clp1* even before zygotic implantation; however, mice with a homozygous kinase-dead mutant allele (p.K127A) survived embryogenesis but died perinatally with spinal motor neuron degeneration (Hanada et al., 2013). To test for central nervous system requirements in a model vertebrate, we generated a germline *clp1* p.R44X mutation by ENU mutagenesis in zebrafish and bred to homozygosity. Wild type fish showed strong neural *clp1* expression by *in situ* hybridization (ISH), which was severely reduced in mutants (Figure S3A). Heterozygous and wt clutchmates were indistinguishable, but homozygous mutants did not survive past 5 days post fertilization (dpf), displayed abnormal swimming behavior, abnormal head shape and curved tail consistent with a neuromotor defect (Figure 3A-B). A second allele, representing a missense mutation near the kinase domain (p.L35R) showed a similar uniform lethality by 5 dpf (Figure S3B). We conclude that *clp1* is essential in zebrafish.

From timed larvae, whole mount ISH for the midbrain marker, *otx2*, demonstrated unremarkable expression level and distribution at 24 hours post-fertilization (hpf) in mutants (Figure 3C). However, by 48 hpf mutants displayed weak, spatially restricted expression of *otx2*, and by 72 hpf, *otx2* was not evident in the mutant zebrafish. Since initial *otx2* expression was initially unremarkable in mutant animals, our data suggests the progressive loss of expression results from cell loss as opposed to defective patterning. To further differentiate between these possibilities, we performed terminal deoxynucleotidyl transferase dUTP nick end labeling (TUNEL), to detect DNA fragmentation (Chen et al., 2010). We noted a dramatic increase in staining specific to the forebrain and hindbrain (Figure 3D). Therefore, *clp1* mutant zebrafish showed evidence of hindbrain neurodegeneration, similar to *tsen54* zebrafish morphant (Kasher et al., 2011). The similarity in brain phenotype between the human p.R140H and the zebrafish mutations suggests loss-of-function as the disease mechanism in humans.

We next tested for a spinal motor neuron phenotype, since both mouse and human show loss of this class of neurons with *CLP1* mutations. Zebrafish larvae were fixed at 72 hpf and stained with the motor neuron marker Sv2 (Boon et al., 2009). Specifically in the *clp1* p.R44X mutants, we found altered motor neuron morphology with full penetrance (Figure S3C), similar to established zebrafish motor neuron mutants (Fassier et al., 2010).

In mouse, multiple phenotypes observed in *Clp1* mutants are rescued by allelic removal of *p53*, suggesting that the cellular apoptosis observed in *clp1* mutants is p53-dependent (Hanada et al., 2013). In order to test this in zebrafish, we performed *p53* morpholino knockdown using a published reagent (Langheinrich et al., 2002) in *clp1* wt and mutants, then performed *otx2* ISH as a marker for cell loss. We observed rescued *otx2* expression in *p53*-knockdown *clp1* mutant zebrafish, suggesting the neural apoptosis is p53-dependent

(Figure S3D). We also performed zygotic knockdown of the single *hspc117* zebrafish orthologue, the gene proposed to mediate the redundant splicing pathway, with either ATG- or splice-blocking morpholinos, achieving near complete loss of spliced transcript with the latter. However, we found no phenotype in any of the morphants (not shown). We additionally performed *hspc117* knockdown in *clp1* p.R44X mutants, but found no exacerbation of the *clp1* mutant phenotype (not shown), suggesting that, at least in zebrafish, *hspc117* does not play an essential role, or genetically interact with *clp1*.

To determine if human *CLP1* is a functional orthologue of zebrafish *clp1* we injected wt and mutant human *CLP1* mRNA into mutant *clp1* p.R44X mutant fish zygotes. The curved tail phenotype was apparent by 48 hpf so we utilized this as a readout as measured by the depth of the vertebral curve from highest to lowest point at 3 dpf. Average height was less than 50 μm in wt fish but over 300 μm in mutant fish (Figure 3E). Injection of wt human *CLP1* mRNA partially rescued the average curve height to less than 200 μm, although variable from fish-to-fish. Injection of the human p.R140H mutant *CLP1* mRNA did not mediate such rescue, with peak average height not less than 300 μm. In addition, we performed ISH for *otx2* on wt and *clp1* p.R44X mutants injected with human *CLP1* mRNA. As expected, human wt *CLP1*, but not $CLP1^{R140H}$ was sufficient to prevent most loss of *otx2* expression in *clp1* p.R44X mutants (Figure 3F). We conclude that human *CLP1* can at least partially replace the zebrafish *clp1*, suggesting the human and zebrafish *CLP1* genes are orthologues, and that the human mutation lacks activity *in vivo*.

Patient $CLP1^{R140H}$ iNeurons show intron-containing pre-tRNAs accumulation and mature tRNA depletion

Due to the shared hindbrain phenotype observed in zebrafish and the established role of the TSEN/CLP1 complex in tRNA splicing, we pursued defective tRNA splicing as a potential disease mechanism. In order to study the relative expression of the known 32 intron-containing tRNA isoforms (i.e. genes), following reverse transcription (RT) of total RNA, we generated isoform-specific pre-tRNA primers to each, utilizing the unique intronic sequence for the reverse primer (Figure 4A). Excluding those that failed PCR or where expression was undetectable, using RT-PCR we profiled the expression of the remaining 15 in human cortex, iNeurons, and fibroblasts (Figure S4A). Expression in brain more closely mirrored expression in iNeurons than fibroblasts, supporting the use of iNeurons for these experiments.

To test for defective tRNA splicing, we generated cDNA from fibroblasts and iNeurons, then analyzed expression of these pre-tRNAs using qRT-PCR to test for differences between affected and unaffected. Normalizing to the unaffected in fibroblasts, in the half of pre-tRNAs where a difference was noted, the differences were roughly equally distributed into those where the pre-tRNA was higher in the affected and those where it was lower in the affected (Figure 4B, S4B). In iNeurons, however, where a difference in pre-tRNAs level was noted, the majority (6 of 8) showed an accumulation of pre-tRNA in affected cells compared with unaffected (Figure 4C, S4C). We conclude that there is an accumulation of some pre-tRNAs in *CLP1* patient cells.

To exclude that the qPCR data was biased due to impaired RT of fully modified tRNAs, we utilized Northern blotting, the most established method for tRNA assessment, generating probes to interrogate representative unique isoforms for pre-tRNA for Tyrosine Chr14:tRNA19 and Isoleucine Chr19:tRNA10, as well as to detect all isoacceptor (pan: all isoacceptor, i.e. same anticodon) for pre-tRNA and mature tRNA for Tyrosine, Isoleucine and Leucine. Most probes showed some evidence for expression in both fibroblasts and iNeurons with the exception of pre-tRNA for Chr14:tRNA19-TyrGTA, which was detectable only in iNeurons, run in duplicate to avoid sample loading variability. We identified both accumulation of pre-tRNAs as well as depletion of mature tRNAs specifically in patient iNeurons. Pre-tRNA Chr14:tRNA19-TyrGTA, pre-tRNA Chr19:tRNA10-IleTAT, as well as pre-tRNA IleTAT (pan) and pre-tRNA LeuCAA (pan) showed stronger bands in affected vs. unaffected iNeurons (Figure 4D). We also noted an accumulation of Chr19.tRNA10-IleTAT intron (data not shown). Correspondingly, there was a reduction in the amounts of mature tRNAs for Isoleucine and Leucine for mature tRNA IleTAT (pan) and mature tRNA LeuCAA (pan). These results were quantified as the percent mature tRNA or pre-tRNA of total tRNA for each isoacceptor, and demonstrate neural specific changes in pre- and mature tRNA transcript levels.

Next we analyzed whether the alterations in pre-tRNA levels were due to impaired TSEN-CLP1 complex formation resulting from the *CLP1* p.R140H mutation. Using an established assay (Figure S4D) (Paushkin et al., 2004), we found reduced amounts of the active site containing TSEN complex proteins, TSEN2 and TSEN34 co-purified with double-affinity tagged CLP1^{R140H}, compared to complexes purified with wt CLP1 or TSEN54 (Figure 4E, S4E). Additionally, we generated two control mutants, CLP1^{R140A} and CLP1^{K127A}, and observed a less severe reduction of TSEN2 and TSEN34 bound compared to CLP1^{R140H}, indicating the patient substitution p.140H is particularly damaging to TSEN complex formation (Figure 4E, S4E) (Hanada et al., 2013). We conclude that mutant CLP1 has altered affinity for the TSEN complex.

To determine if CLP1^{R140H}-, CLP1^{R140A}- and CLP1^{K127A}-bound protein complexes display altered endonuclease activity we performed an *in vitro* tRNA cleavage assay using the co-purified protein complexes isolated from the two step elution (Figure S4D) and radiolabeled Tyrosine pre-tRNA with yeast tRNA endonuclease as a positive enzymatic control (Trotta et al., 2006). Consistent with a severe defect in TSEN complex affinity, CLP1^{R140H}-associated protein complexes were unable to cleave pre-tRNA Tyr as compared to wt CLP1-purified complexes at all time points analyzed (Figure 4F). As expected, CLP1^{R140A} and CLP1^{K127A} co-purified complexes displayed more endonuclease activity than CLP1^{R140H}-bound proteins, but less activity than wt (Figure S4F). The data suggest that loss of the TSEN complex from mutant CLP1-associated protein complexes impairs pre-tRNA cleavage activity.

The Tyr tRNA 5'-Phospho-3'-exon fragment protects *CLP1^{R104H}* mutant cells from stress-induced cell death

As there are at least two proposed mechanisms of re-ligating "half" tRNAs in mammals we set out to uncover the requirement for CLP1 in human cells. To test for altered cell viability

of *CLP1* mutant cells, we performed growth analysis of fibroblasts and iNeurons under basal conditions, but detected no differences (Figure S5A-B). We next tested whether overexpression of pre-tRNAs compared with mature tRNAs were toxic in patient iNeurons in culture, since iNeurons displayed an accumulation of these pre-tRNAs. Using a lentiviral delivery system expressing Chr14:tRNA19-TyrGTA or Chr19:tRNA10-IleTAT pre- or processed tRNA (both pre isoforms accumulated by Northern analysis in patient iNeurons), we found no difference in viability between patient and control iNeurons 24h after transduction (Figure S5C). We conclude that the patient iNeurons do not show a dose-dependent toxicity to pre-tRNAs under these conditions.

Oxidative stress can up-regulate tRNA cleavage (Thompson et al., 2008). We detected no differences in basal protein or DNA oxidation in patient fibroblasts or iNeurons compared with controls, but noted that iNeurons showed higher basal oxidation than fibroblasts, irrespective of genotype (Figure S5D-E). Therefore to determine whether $CLP1^{R140H}$ patient cells display heightened sensitivity to oxidative stress-induced cell death, we performed a dose-dependent cell viability assay using hydrogen peroxide. (HP). As previously reported in murine fibroblasts (Hanada et al., 2013), we found that human $CLP1^{R140H}$ mutant fibroblasts and iNeurons showed compromised cell survival to HP at the highest 50 uM concentration, indicating sensitivity to oxidative stress (Figure S5F-G).

It was recently proposed that excessive 5’-half-tRNAs were responsible for p53-dependent activation of cellular stress in mice (Hanada et al., 2013). Therefore, we hypothesized that inadequate CLP1 kinase activity might result in 3’-half-tRNAs that lacked a phospho group at the 5’-end (Figure 5A). We used a stress-induced viability assay to determine whether the patient mutation affected cell survival in the presence of various tRNA fragments, testing whether the addition of 3’- or 5’-half-tRNA fragments might exacerbate the HP-induced phenotype in human cells. We predicted that the substrate but not the product of CLP1 modification (i.e. the unphosphorylated but not the phosphorylated 3’-exon) would be toxic.

We transfected control and $CLP1^{R140H}$ mutant fibroblasts with RNA oligonucleotides corresponding to the most abundantly expressed Tyr tRNA intermediates, either in the absence or presence of HP and evaluated cell viability after 24h (Figure 5B-C). Control fibroblasts and neural progenitor cells showed little toxicity in response to the tRNA intermediates, either in the absence or presence of HP (Figure S5H-I, K). Co-treatment with the 5’-exon containing the terminal 2’-3’-cyclic phosphodiester did not have a notable effects on survival (Figure S5H). Most strikingly, the unphosphorylated 3’-exon was the most lethal of the tRNA halves, particularly in the presence of HP (Figure 5B, S5I). Remarkably, the 5’-phosphorylated 3’-exon did not cause toxicity and in fact significantly improved viability in the presence of HP (Figure 5C, S5J). These results are consistent with the model whereby the loss of the phosphorylated-3’-exon required for HSPC117-independent tRNA ligation (and therefore production of mature tRNAs) or the toxic hydroxyl-3’-exon (incapable of further processing in mutant cells), may contribute significantly to the disease phenotype in patients.

DISCUSSION

Our results provide the first report of the effect of a *CLP1* mutation in humans. Based upon this, and previously published data, we propose that patients with a *CLP1*^{R140H} founder mutation display neurodegeneration due to defects in tRNA splicing. Because CLP1, in at least one capacity, associates with the TSEN complex and because patients display features similar to PCH, we propose that the condition we describe here should be considered a new form of PCH that we propose as PCH type 10. The appearance of the brain scan is very distinct from the previously published PCH forms, does not show the “dragonfly” sign (Namavar et al., 2011a), and shows equal involvement of the hindbrain and forebrain. Further characterization of this clinical phenotype could help better define similarities/differences from other forms of PCH.

While CLP1 kinase-dead mice develop progressive loss of spinal motor neurons mimicking the pathology of amyotrophic lateral sclerosis, our patients showed instead a neurodegenerative disease with loss of cerebellar, brainstem and cortical volume, thinning of the corpus callosum, and loss of acquired motor and cognitive skills, with evidence for later loss of motor neurons. Certain forms of PCH show co-existent spinal motor neuron degeneration, notably PCH type I (also known as Norman's disease), and PCH due to *EXOCS3* mutations (Goutieres et al., 1977; Wan et al., 2012), suggesting that both hindbrain and motor neurons may share susceptibility across the mutation spectrum. Cerebellar Purkinje cells and spinal motor neurons are among the largest neurons and thus likely most metabolically challenged of the cells in the nervous system, but why these specific neuronal cell types are vulnerable to reduced CLP1 activity is unclear.

The CLP1 p.R140H mutation does not destabilize the protein, but substantially impairs kinase activity, alters the nuclear localization, reduces the affinity for TSEN proteins affecting tRNA endonuclease activity, and when expressed in *Clp1* mutant zebrafish, fails to rescue *in vivo* phenotypes. In an accompanying manuscript in this issue of *Cell* (Karaca et al., 2014), show similar biochemical findings in addition to evidence of microcephaly in *Clp1*-kinase dead mice. Together, our findings support a mechanism by which the patient mutation impacts several of the known functions of CLP1.

In this study, we focus on the role of CLP1 in tRNA processing and show elevated levels of some unspliced pre-tRNAs and depletion of some mature tRNAs for several different isoacceptors including Tyrosine, Isoleucine and Leucine in iNeurons. This result implies reduced processivity of pre-tRNAs to mature tRNAs when *CLP1* is mutated, which we predict occurs at both the pre-tRNA cleavage step and the ligation step directly downstream of CLP1 in the processing cascade. The presence of the HSPC117 redundant splicing pathway may account for the rescue of processed tRNA levels in the presence of the *CLP1* mutation in fibroblasts, although we found no phenotype upon *hspc117* knockdown in fish, and no genetic interaction with *clp1*. Thus the relative contributions of the two tRNA splicing pathways, or others yet undefined, will require further investigation.

A reduction in tRNA ligation results in the accumulation of tRNA half fragments, which inhibit protein translation and cause cell death in yeast and mammalian cells (Sobala and

Hutvagner, 2013; Thompson et al., 2008; Thompson and Parker, 2009; Yamasaki et al., 2009). The CLP1 kinase-dead mice accumulated a 5'-tRNA exon derivative fragment, but we found no evidence of accumulation or toxicity of this fragment in human cells. Instead, we found that unphosphorylated 3'-exon (i.e. a substrate for CLP1) but not the phosphorylated 3'-exon exacerbated toxicity. Our findings support a required role for CLP1 in the 5'-end phosphorylation-dependent ligation of "half"-tRNAs in humans. Cumulatively, we uncover a cell-type specific requirement for the HSPC117-independent tRNA maturation pathway in human development, which when perturbed causes a new PCH-like neurological disease.

In addition to the tRNA processing defects described here, the combined effect of the CLP1 loss-of-function phenotypes may be due to impaired phosphorylation of target RNA. In particular, CLP1 functions as an siRNA kinase required for loading siRNA onto the RISC complex (Weitzer and Martinez, 2007), and thus there may be other cellular effects on these pathways as a result of the mutation. CLP1 also functions as part of a multi-protein complex required for 3'-end cleavage in pre-mRNA processing and maturation (de Vries et al., 2000; Wickens and Gonzalez, 2004), and not surprisingly we observed $CLP1^{R140H}$-bound protein complexes were depleted of mRNA 3'-end processing proteins (data not shown). Further experimentation will be required to test whether these other cellular mechanisms contribute to the disease pathogenesis in these patients.

EXPERIMENTAL PROCEDURES

Methods and any associated references are available in the online version of the paper at http://www.cell.com

Patient Recruitment

Patients were enrolled and sampled by standard practice in approved human subjects protocols at the University of California, San Diego.

Exome Sequencing

Genomic DNA was extracted and subjected to exon capture, sequencing, variant identification, and computational filtering as previously described (Akizu et al., 2013). See Extended Experimental Procedures for more detail.

Zebrafish

Zebrafish work was performed in accordance with AMC IACUC regulations. ENU mutagenesis was performed to create two independent *clp1* mutations. Gene knockdown was performed with morpholino oligonucleotides (Gene-Tools). Lifespan analysis, *in situ* hybridization, TUNEL, RNA rescue, and immunostaining were performed with standard protocols. Additional detail can be found in the Extended Experimental Procedures.

tRNA analysis

RNA from patient fibroblasts or iNeurons was used for cDNA generation and quantitative RT-PCR of pre-tRNAs using standard methods. Northern blot for intron containing pre- and

mature tRNAs were assessed by standard protocols. Probe and primer sequences, and detailed protocols are listed in the Extended Experimental Procedures.

Cell Culture

Fibroblasts were generated from Unaffected and Affected skin punch biopsies. Induced Neurons (iNeurons) were generated as previously described (Xue et al., 2013). HEK293T, HEK293H, primary fibroblasts, neural progenitor cells, and iNeurons were cultures using well-established techniques. Basal protein and DNA oxidation and RNA transfection were performed as suggested by the manufacturer. Cell viability assays were performed as previously described (Carmichael et al., 1987). Details can be found in the Extended Experimental Procedures.

CLP1 Protein Assays

Recombinant wt and mutant GST-CLP1 was purified from *E. coli* and tested for kinase activity as previously described (Ramirez et al., 2008). Double affinity purification of FlagHis-CLP1 was carried out as previously described (Trotta et al., 2006; Volta et al., 2005). Associated protein complexes were used in tRNA endonuclease assays and analyzed by Western blot. Detailed experimental techniques can be found in the Extended Experimental Procedures.

Computation

CLP1 mutations were modeled onto the crystalized yeast structure with Phyre2 (Kelley and Sternberg, 2009). PLINK was used to create autozygosity maps from exome sequence (Purcell et al., 2007). The age of the CLP1 p.R140H mutation was calculated according to published methods (Fu et al., 2013). Additional details can be found in the Extended Experimental Procedures.

Statistical Analysis

ANOVA (1- or 2-way) or Student's two-tailed non-paired *t* tests were carried out to determine the statistical significance of differences between samples. $P < 0.05$ was considered nominally statistically significant for all tests.

Supplementary Material

Refer to Web version on PubMed Central for supplementary material.

Acknowledgments

Supported by the NIH (P01HD070494, R01NS048453, and P30NS047101 for imaging support to J.G.G., Broad Institute grant U54HG003067 to Eric Lander, GM049369 to X.-D.F., the Yale Center for Mendelian Disorders U54HG006504 to R. Lifton and M.G., RC2NS070477), the Gregory M. Kiez and Mehmet Kutman Foundation to M.G. We acknowledge M. Gerstein, S. Mane, A. B. Ekici, ad S. Uebe for sequencing support and analysis, the Yale Biomedical High Performance Computing Center for data analysis and storage, the Yale Program on Neurogenetics, and the Yale Center for Human Genetics and Genomics, the Center for Inherited Disease Research for genotyping; the Simons Foundation Autism Research Initiative. Consortium for Autosomal Recessive Intellectual Disability (CARID) supported patient ascertainment. E.W.E. Verweij for zebrafish analysis, E. Cuppen and H. van Roekel for support with ENU Tilling, and ZF Health funding for tilling. A.E.S. is the recipient of an A.P. Gianinni Fellowship. V.C. was supported by the French National Research Agency (ANR-RVP13016KKA).

J.G.G. is an Investigator of the Howard Hughes Medical Institute. We thank patients and parents for participation, and J. Lupski, J. Martinez and S. Weitzer for communicating unpublished results and sharing reagents.

REFERENCES

Adzhubei IA, Schmidt S, Peshkin L, Ramensky VE, Gerasimova A, Bork P, Kondrashov AS, Sunyaev SR. A method and server for predicting damaging missense mutations. Nat Methods. 2010; 7:248–249. [PubMed: 20354512]

Akizu N, Cantagrel V, Schroth J, Cai N, Vaux K, McCloskey D, Naviaux RK, Van Vleet J, Fenstermaker AG, Silhavy JL, et al. AMPD2 regulates GTP synthesis and is mutated in a potentially treatable neurodegenerative brainstem disorder. Cell. 2013; 154:505–517. [PubMed: 23911318]

Boon KL, Xiao S, McWhorter ML, Donn T, Wolf-Saxon E, Bohnsack MT, Moens CB, Beattie CE. Zebrafish survival motor neuron mutants exhibit presynaptic neuromuscular junction defects. Hum Mol Genet. 2009; 18:3615–3625. [PubMed: 19592581]

Budde BS, Namavar Y, Barth PG, Poll-The BT, Nurnberg G, Becker C, van Ruissen F, Weterman MA, Fluiter K, te Beek ET, et al. tRNA splicing endonuclease mutations cause pontocerebellar hypoplasia. Nat Genet. 2008; 40:1113–1118. [PubMed: 18711368]

Carmichael J, DeGraff WG, Gazdar AF, Minna JD, Mitchell JB. Evaluation of a tetrazolium-based semiautomated colorimetric assay: assessment of chemosensitivity testing. Cancer Res. 1987; 47:936–942. [PubMed: 3802100]

Chen HL, Yuh CH, Wu KK. Nestin is essential for zebrafish brain and eye development through control of progenitor cell apoptosis. PLoS ONE. 2010; 5:e9318. [PubMed: 20174467]

de Vries H, Ruegsegger U, Hubner W, Friedlein A, Langen H, Keller W. Human pre-mRNA cleavage factor II(m) contains homologs of yeast proteins and bridges two other cleavage factors. Embo J. 2000; 19:5895–5904. [PubMed: 11060040]

DePristo MA, Banks E, Poplin R, Garimella KV, Maguire JR, Hartl C, Philippakis AA, del Angel G, Rivas MA, Hanna M, et al. A framework for variation discovery and genotyping using next-generation DNA sequencing data. Nat Genet. 2011; 43:491–498. [PubMed: 21478889]

Edvardson S, Shaag A, Kolesnikova O, Gomori JM, Tarassov I, Einbinder T, Saada A, Elpeleg O. Deleterious mutation in the mitochondrial arginyl-transfer RNA synthetase gene is associated with pontocerebellar hypoplasia. Am J Hum Genet. 2007; 81:857–862. [PubMed: 17847012]

Fassier C, Hutt JA, Scholpp S, Lumsden A, Giros B, Nothias F, Schneider-Maunoury S, Houart C, Hazan J. Zebrafish atlastin controls motility and spinal motor axon architecture via inhibition of the BMP pathway. Nat Neurosci. 2010; 13:1380–1387. [PubMed: 20935645]

Fu W, O'Connor TD, Jun G, Kang HM, Abecasis G, Leal SM, Gabriel S, Rieder MJ, Altshuler D, Shendure J, et al. Analysis of 6,515 exomes reveals the recent origin of most human protein-coding variants. Nature. 2013; 493:216–220. [PubMed: 23201682]

Goutieres F, Aicardi J, Farkas E. Anterior horn cell disease associated with pontocerebellar hypoplasia in infants. J Neurol Neurosurg Psychiatry. 1977; 40:370–378. [PubMed: 874513]

Hanada T, Weitzer S, Mair B, Bernreuther C, Wainger BJ, Ichida J, Hanada R, Orthofer M, Cronin SJ, Komnenovic V, et al. CLP1 links tRNA metabolism to progressive motor-neuron loss. Nature. 2013; 495:474–480. [PubMed: 23474986]

Karaca E, Weitzer S, Pehlivan D, Shiraishi H, Gogakos T, Hanada T, Wiszniewski W, Withers M, Campbell IM, Erdin S, et al. Human CLP1 mutations alter tRNA biogenesis affecting both peripheral and central nervous system function. Cell. 2014 in press.

Kasher PR, Namavar Y, van Tijn P, Fluiter K, Sizarov A, Kamermans M, Grierson AJ, Zivkovic D, Baas F. Impairment of the tRNA-splicing endonuclease subunit 54 (tsen54) gene causes neurological abnormalities and larval death in zebrafish models of pontocerebellar hypoplasia. Hum Mol Genet. 2011; 20:1574–1584. [PubMed: 21273289]

Kelley LA, Sternberg MJ. Protein structure prediction on the Web: a case study using the Phyre server. Nat Protoc. 2009; 4:363–371. [PubMed: 19247286]

Langheinrich U, Hennen E, Stott G, Vacun G. Zebrafish as a model organism for the identification and characterization of drugs and genes affecting p53 signaling. Curr Biol. 2002; 12:2023–2028. [PubMed: 12477391]

Lowe TM, Eddy SR. tRNAscan-SE: a program for improved detection of transfer RNA genes in genomic sequence. Nucleic Acids Res. 1997; 25:955–964. [PubMed: 9023104]

Namavar Y, Barth PG, Kasher PR, van Ruissen F, Brockmann K, Bernert G, Writzl K, Ventura K, Cheng EY, Ferriero DM, et al. Clinical, neuroradiological and genetic findings in pontocerebellar hypoplasia. Brain. 2011a; 134:143–156. [PubMed: 20952379]

Namavar Y, Barth PG, Poll-The BT, Baas F. Classification, diagnosis and potential mechanisms in pontocerebellar hypoplasia. Orphanet J Rare Dis. 2011b; 6:50. [PubMed: 21749694]

Noble CG, Beuth B, Taylor IA. Structure of a nucleotide-bound Clp1-Pcf11 polyadenylation factor. Nucleic Acids Res. 2007; 35:87–99. [PubMed: 17151076]

Paushkin SV, Patel M, Furia BS, Peltz SW, Trotta CR. Identification of a human endonuclease complex reveals a link between tRNA splicing and pre-mRNA 3′ end formation. Cell. 2004; 117:311–321. [PubMed: 15109492]

Peebles CL, Gegenheimer P, Abelson J. Precise excision of intervening sequences from precursor tRNAs by a membrane-associated yeast endonuclease. Cell. 1983; 32:525–536. [PubMed: 6186398]

Phizicky EM, Hopper AK. tRNA biology charges to the front. Genes Dev. 2010; 24:1832–1860. [PubMed: 20810645]

Popow J, Englert M, Weitzer S, Schleiffer A, Mierzwa B, Mechtler K, Trowitzsch S, Will CL, Luhrmann R, Soll D, et al. HSPC117 is the essential subunit of a human tRNA splicing ligase complex. Science. 2011; 331:760–764. [PubMed: 21311021]

Purcell S, Neale B, Todd-Brown K, Thomas L, Ferreira MA, Bender D, Maller J, Sklar P, de Bakker PI, Daly MJ, et al. PLINK: a tool set for whole-genome association and population-based linkage analyses. Am J Hum Genet. 2007; 81:559–575. [PubMed: 17701901]

Ramirez A, Shuman S, Schwer B. Human RNA 5'-kinase (hClp1) can function as a tRNA splicing enzyme in vivo. RNA. 2008; 14:1737–1745. [PubMed: 18648070]

Renbaum P, Kellerman E, Jaron R, Geiger D, Segel R, Lee M, King MC, Levy-Lahad E. Spinal muscular atrophy with pontocerebellar hypoplasia is caused by a mutation in the VRK1 gene. Am J Hum Genet. 2009; 85:281–289. [PubMed: 19646678]

Seelow D, Schuelke M, Hildebrandt F, Nurnberg P. HomozygosityMapper--an interactive approach to homozygosity mapping. Nucleic Acids Res. 2009; 37:W593–599. [PubMed: 19465395]

Sobala A, Hutvagner G. Small RNAs derived from the 5′ end of tRNA can inhibit protein translation in human cells. RNA biology. 2013; 10:553–563. [PubMed: 23563448]

Thompson DM, Lu C, Green PJ, Parker R. tRNA cleavage is a conserved response to oxidative stress in eukaryotes. RNA. 2008; 14:2095–2103. [PubMed: 18719243]

Thompson DM, Parker R. The RNase Rny1p cleaves tRNAs and promotes cell death during oxidative stress in Saccharomyces cerevisiae. J Cell Biol. 2009; 185:43–50. [PubMed: 19332891]

Trotta CR, Paushkin SV, Patel M, Li H, Peltz SW. Cleavage of pre-tRNAs by the splicing endonuclease requires a composite active site. Nature. 2006; 441:375–377. [PubMed: 16710424]

Volta V, Ceci M, Emery B, Bachi A, Petfalski E, Tollervey D, Linder P, Marchisio PC, Piatti S, Biffo S. Sen34p depletion blocks tRNA splicing in vivo and delays rRNA processing. Biochem Biophys Res Commun. 2005; 337:89–94. [PubMed: 16188229]

Wan J, Yourshaw M, Mamsa H, Rudnik-Schoneborn S, Menezes MP, Hong JE, Leong DW, Senderek J, Salman MS, Chitayat D, et al. Mutations in the RNA exosome component gene EXOSC3 cause pontocerebellar hypoplasia and spinal motor neuron degeneration. Nat Genet. 2012; 44:704–708. [PubMed: 22544365]

Weitzer S, Martinez J. The human RNA kinase hClp1 is active on 3′ transfer RNA exons and short interfering RNAs. Nature. 2007; 447:222–226. [PubMed: 17495927]

Wickens M, Gonzalez TN. Molecular biology. Knives, accomplices, and RNA. Science. 2004; 306:1299–1300. [PubMed: 15550648]

Xue Y, Ouyang K, Huang J, Zhou Y, Ouyang H, Li H, Wang G, Wu Q, Wei C, Bi Y, et al. Direct conversion of fibroblasts to neurons by reprogramming PTB-regulated microRNA circuits. Cell. 2013; 152:82–96. [PubMed: 23313552]

Yamasaki S, Ivanov P, Hu GF, Anderson P. Angiogenin cleaves tRNA and promotes stress-induced translational repression. J Cell Biol. 2009; 185:35–42. [PubMed: 19332886]

Zillmann M, Gorovsky MA, Phizicky EM. Conserved mechanism of tRNA splicing in eukaryotes. Mol Cell Biol. 1991; 11:5410–5416. [PubMed: 1922054]

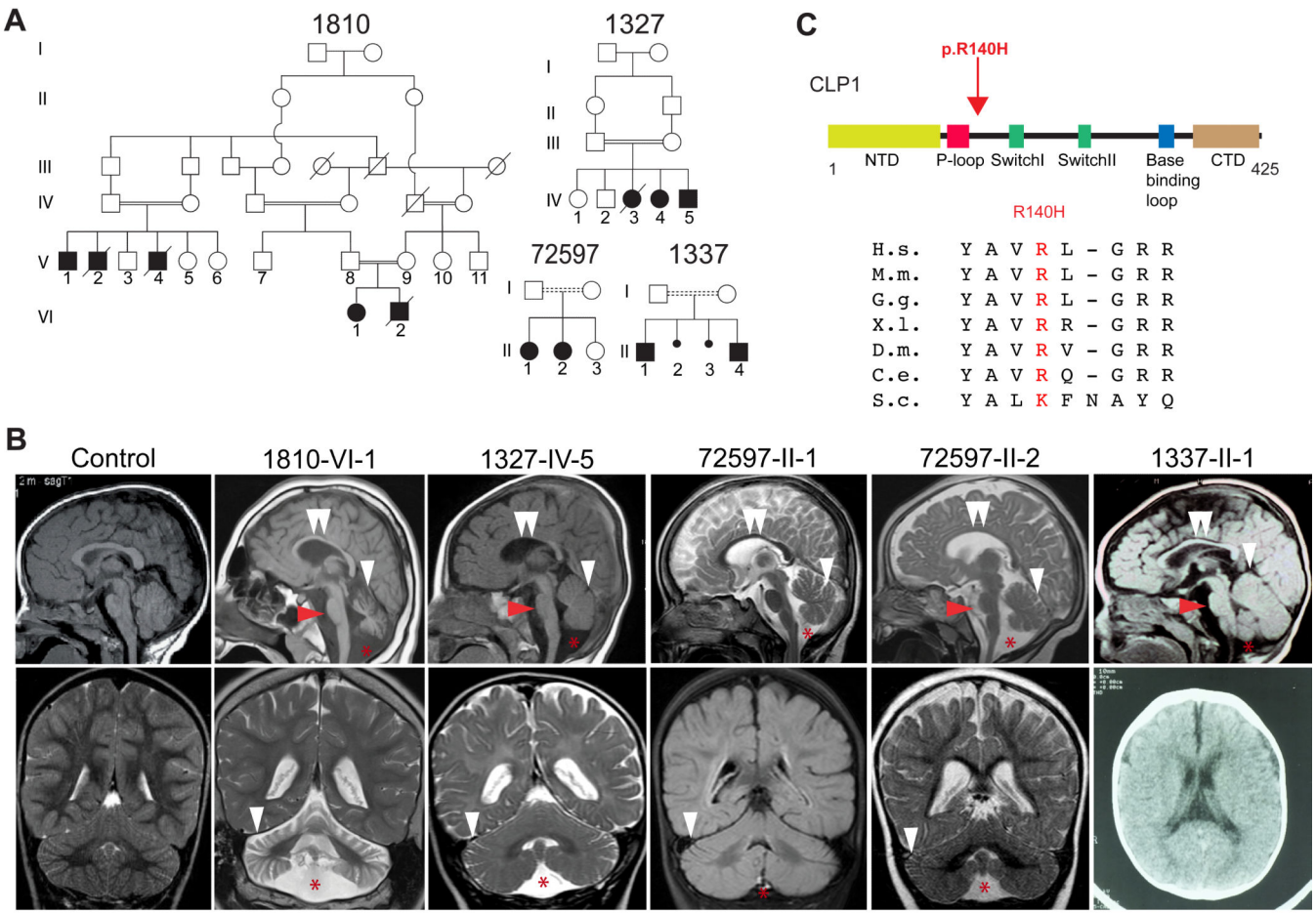

Figure 1.

Identification of a homozygous *CLP1* p.R140H mutation in families with degeneration/hypoplasia of the central nervous system. Further analysis in Figure S1. (A) Pedigrees of four consanguineous Turkish families. Filled symbols: affecteds; hash: deceased; double bar: consanguinity; dashed double bar: history of consanguinity but ancestry not established. (B) Midline sagittal (top) and coronal (bottom) brain MRI of control compared with patients from each family, showing ventriculomegaly due to atrophy. Red arrowhead: hypoplastic/atrophic pons. White arrowhead: cerebellar folia atrophy. Double white arrowheads: hypoplastic corpus callosum. Red asterisk: Fluid cavity as a result of cerebellar atrophy (mega cisterna magna). Only axial CT was available for 1337-II-1. (C) Stick figure of CLP1 protein and location of the p.R140H mutation near the ATP-binding P-loop. Evolutionary conservation of the p.R140 residue across the animal kingdom. NTD: N-terminal domain; P-loop/Walker A motif; Switch loop I; Switch loop II; base-binding loop: involved in nucleotide binding; CTD: C-terminal domain. H.s.: Human; M.m.: Mouse; G.g.: Chicken; X.l.: Frog; D.m.: Fly; C.e.: Worm; S.c.: Yeast.

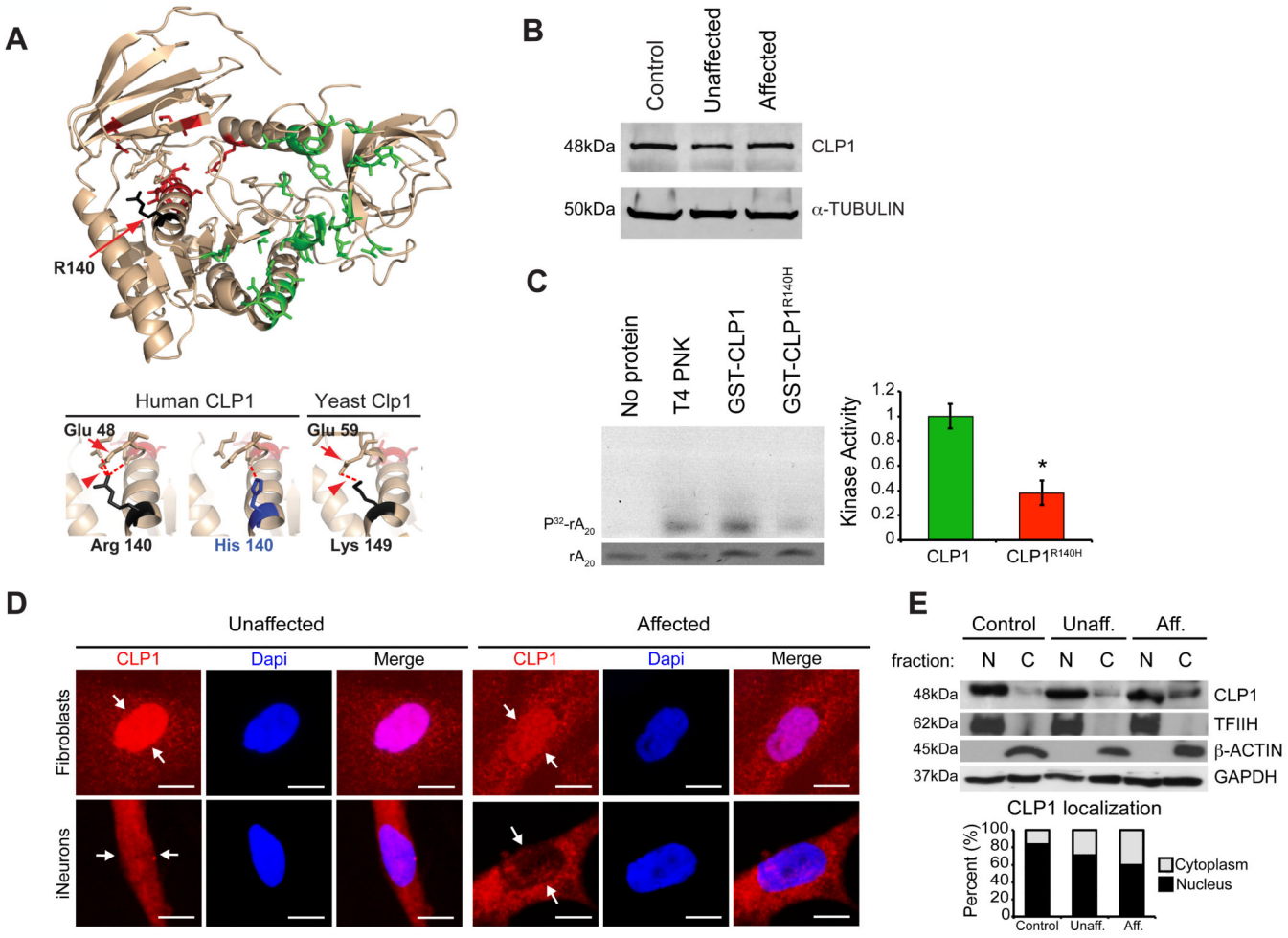

Figure 2.

CLP1 p.R140H is stable but functionally compromised. (A) Homology modeling of human CLP1 with the crystal structure of yeast Clp1 (left). Lower panels: Magnified images of the p.140R and p.140H residues in human and p.149K residue in yeast. Substitution predicted to disrupt conserved hydrogen bond (red arrowhead) formed between p.R140 and GLU (red arrow, residue 48 in human and 59 in yeast). (B) Unaltered levels of CLP1 protein from affected cells. (C) Defective kinase activity of recombinant human CLP1 p.R140H mutation (purification shown in Figure S2), against RNA poly(A)$_{20}$, RNA SYBR staining (bottom), quantified at right. (D) Nuclear localization of CLP1 p.R140H is reduced in affected cells (schematic and validation shown in Figure S2). (E) Western blot of cellular fractions showing CLP1 mislocalization in patient fibroblasts. TFIIH, β-ACTIN, and GAPDH: loading controls, quantified below. N = nuclear, C= cytoplasmic, Unaff. = Unaffected, Aff. = Affected. Error bar: SEM. * $p < 0.05$ Student's *t*-test. Scale bar = 10 μm.

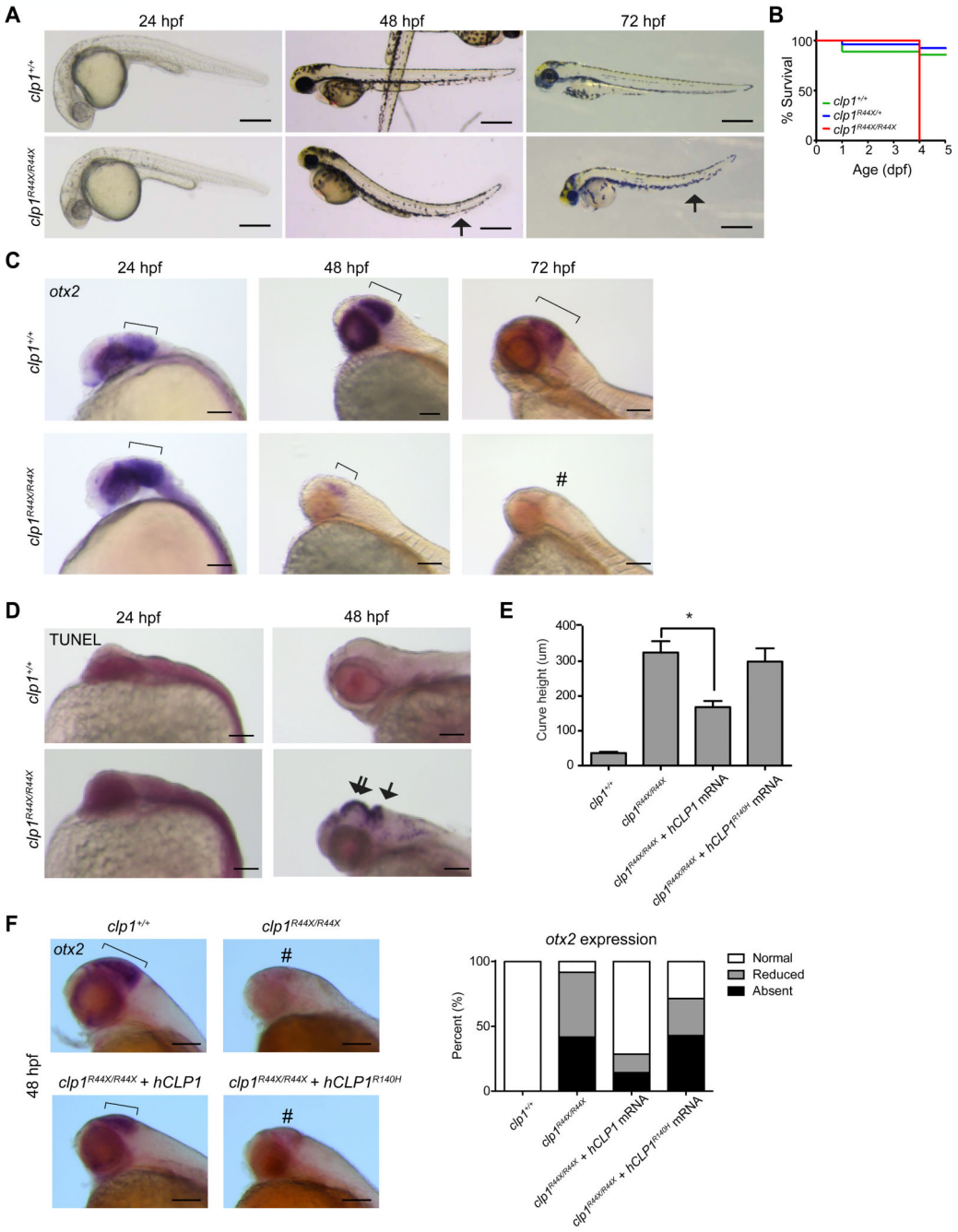

Figure 3.

Zebrafish *clp1*^{R44X} homozygous mutant show gross brain defects, reduced survival and neurodegeneration. (A) Gross morphology of wt and *clp1*$^{R44X/R44X}$ zebrafish mutant showed misshapen head, small eye and curved tail (arrow), suggesting neuromotor defects. Scale bar = 500 μm (B) Kaplan–Meier curve showed reduced survival of *clp1*$^{R44X/R44X}$ fish (additional allele shown in Figure S3). (C) Progressively reduced *otx2* expression in developing *clp1*$^{R44X/R44X}$ zebrafish brains. Broad *otx2* expression domain at 24 hpf was unremarkable in mutant (bracket), suggesting initial patterning was not disrupted. From

48-72 hpf, wt fish showed expression restricted to midbrain-hindbrain organizer (bracket), whereas mutant showed weak expression, completely absent by 72 hpf (#). (D) TUNEL positive cells were dramatically increased in mutant at 48 hpf in both the hindbrain (arrow) and the midbrain/diencephalon (double arrow), further investigated in Figure S3. (E) Partial rescue of the *clp1*$^{R44X/R44X}$ phenotype with human wt but not p.R140H *CLP1* mRNA, by measuring curved tail height. No significance difference was detected between uninjected and injected with p.R140H mRNA, whereas wt mRNA partially recovered curved tail phenotype. p <0.01 student *t*-test. (F) *In situ* for *otx2* in wt, *clp1*$^{R44X/R44X}$, and *clp1*$^{R44X/R44X}$ injected with human *CLP1* mRNA. Human *CLP1*, but not *CLP1*^{R140H}, prevented the loss of *otx2* expression at 48 hpf in *clp1* mutants, quantified at right. n>25 embryos each condition, $p < 0.05$ Student's *t*-test. Scale bar = 100 μm.

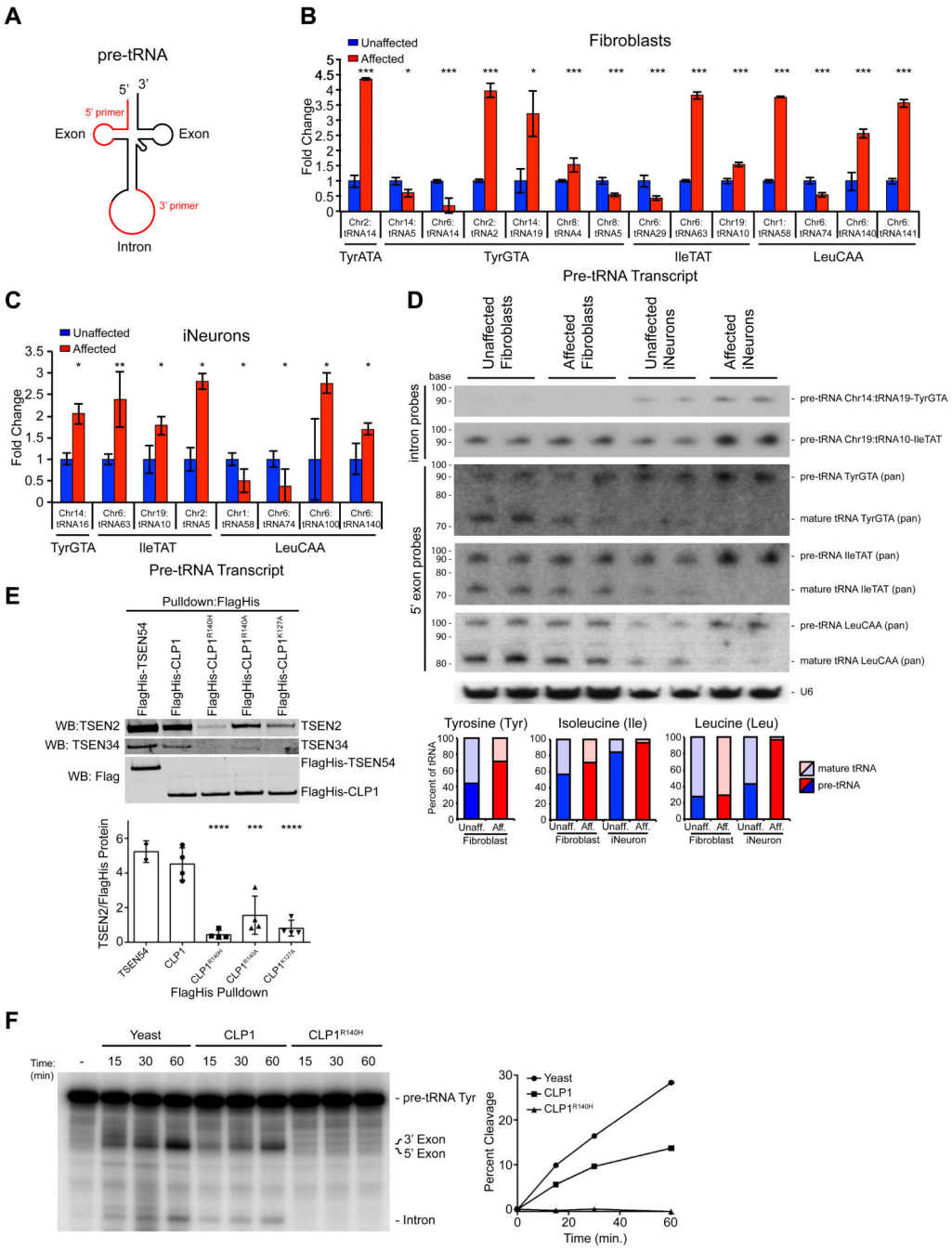

Figure 4.

Increased intron-containing pre-tRNA in *CLP1* mutant patient cells and loss of TSEN complex affinity resulting in reduced pre-tRNA cleavage with CLP1-purified complexes. (A) Schematic pre-tRNA with location of the intron, occurring one base 3’ to the anticodon. Primers designed to the individual tRNA homologue exon sequence and the unique consensus intron (red). Amplifications with the 5’-primer and any of the 3’-primers. (B, C) qRT-PCR results showed variable changes in pre-tRNA expression in Affected fibroblasts (i.e. about half were increased and half were decreased in Affected), while most pre-tRNA

transcripts from Affected iNeurons were increased (i.e. six of eight were increased). Validation and unchanged pre-tRNAs are shown in Figure S4. (D) Northern blot analysis of Chr14:tRNA19-TyrGTA and Chr19:tRNA10-IleTAT pre-tRNA (intron probes) and tRNA-TyrGTA, tRNA-IleTAT, tRNA-LeuCAA pan mature tRNA (5'-exon probes) transcripts relative to U6 loading control, in duplicate showed similar amounts of pre-tRNA and mature tRNA for all transcripts tested, while Affected iNeurons show a increase in Tyr, Ile, and Leu pre-tRNA transcripts, with a corresponding reduction in processed, mature tRNA. Quantification below, displayed as percent mature or pre-tRNA of total tRNA. (E) Western blot of CLP1-purified complexes showing CLP1 p.R140H, p.R140A, and p.K127A with reduced bound TSEN2 and TSEN34 compared to wt CLP1 (TSEN54 served as a positive control). Quantification of the amount of TSEN2 normalized to FlagHis-tagged protein from four independent replicates (below). (F) Time-course of tRNA endonuclease reactions performed on exogenous radiolabeled Tyrosine (Tyr) pre-tRNA with double affinity purified CLP1-bound complexes. Buffer serves as a negative control and Yeast tRNA endonuclease as a positive control. Reduced endonuclease activity observed with $CLP1^{R140H}$ bound complexes compared with wt, quantified at left. *= $p < 0.05$, **= $p < 0.01$, ***= $p < 0.001$, ****= $p < 0.0001$ Students *t*-test (qPCRs) or one-way ANOVA (pulldown).

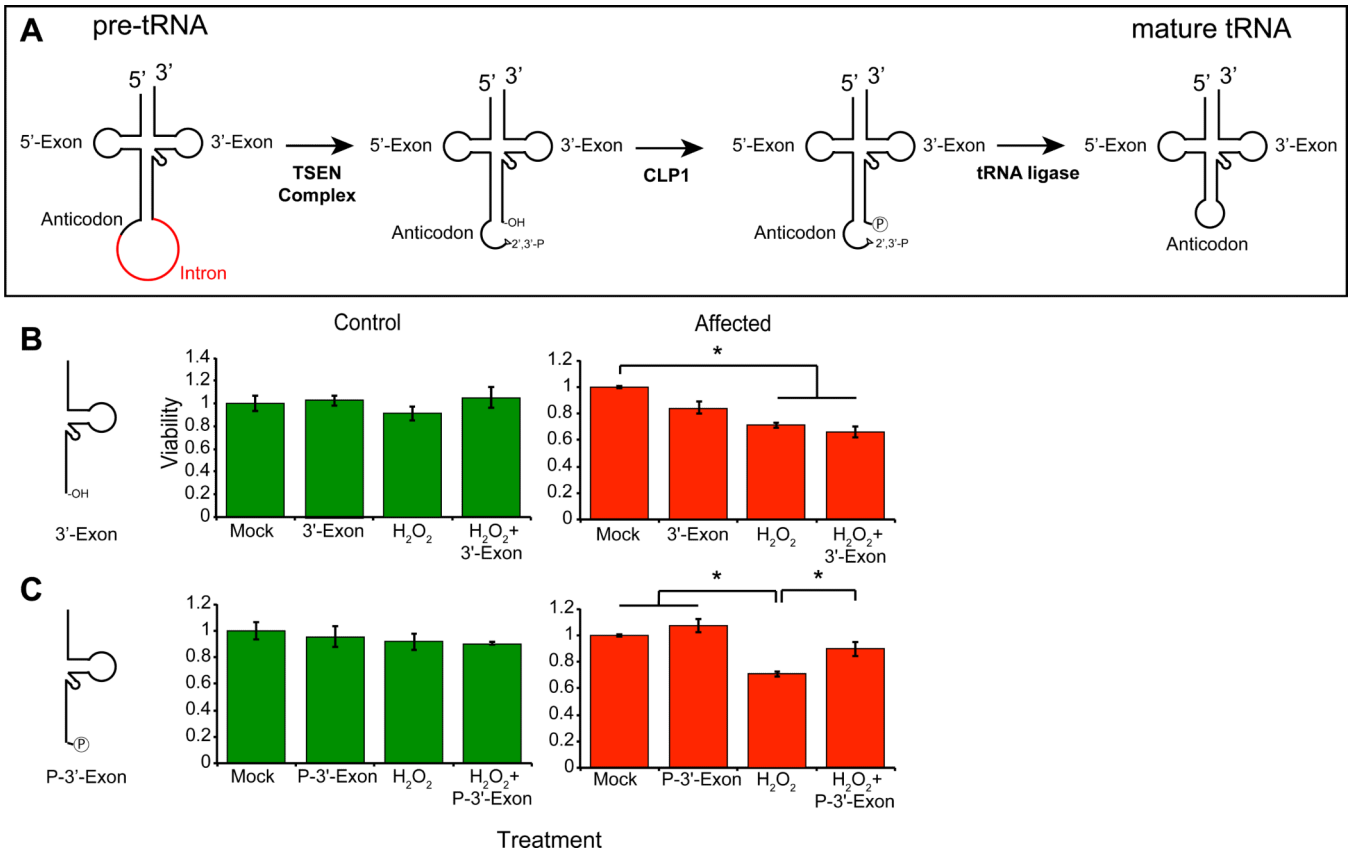

Figure 5.

Toxic effects of unprocessed 3'-"half" tRNA exon in *CLP1* patient cells. (A) Model of tRNA splicing. The pre-tRNA contains an intron (red) 1 base 3' of the anticodon. The TSEN complex excises the intron, leaving two "half" tRNAs, the 5'-exon containing a 2'-3'-phosphodiester, and the 3'-exon containing an hydroxyl group. CLP1 is capable of phosphorylating the 5'-end of the 3'-exon, then a still unknown ligase repairs the break. (B, C) Control (green) and *CLP1* patient cells (red) transfected with either the unphosphorylated 3'-exon (3'-Exon), or the phosphorylated 3'-exon (P-3'-Exon), in the presence or absence of hydrogen peroxide. None of the conditions were adverse to control cells (shown in Figure S5), whereas patient cells showed reduced viability to hydrogen peroxide and 3'-Exon transfection, and improved viability upon P-3'-Exon transfection. * $p < 0.05$ 2-way ANOVA.

Table 1

Clinical phenotypes.

		1810-VI-1	1327-IV-3 (died at 4 yo)	1327-IV-4	1327-IV-5	72597-II-1	72597-II-2	1337-II-1	1337-II-4
Evaluation	**Gender**	F	M	F	M	F	F	M	M
	Ethnic origin	Turkish	Turkish	Turkish	Turkish	Turkish	Turkish	Turkish	Turkish
	Pregnancy duration (weeks)	40	38	N/A	N/A	37	38	38	38
	Polyhydramnios	-	-	N/A	N/A	-	-	-	-
	Weight at birth (kg)	3.5	2.74	N/A	N/A	2.48	3.10	N/A	N/A
	Length at birth (cm)	N/A	49	N/A	N/A	46	51	N/A	N/A
	HC at birth (SD)	−2 SD	−2 SD	−2 SD	N/A	−1/−2 SD	0 SD	0 SD	0 SD
	Diagnosis age	3 yrs	2yrs 9 mos	N/A	N/A	8 yrs	5 yrs	5yrs	6yrs
	HC at latest examination (−SD)	−4 SD	−9/−10 SD	−8 /−9 SD	N/A	−6 SD	−3 SD	−1/−2 SD	−1/−2 SD
	Intellectual disability	+	+	+	+	+	+	+	+
	Irritability	-	-	-	-	-	-	+	+
Seizures	**Seizures**	+	+ (Left temporal)	+	+	+	Febrile (once)	+	-
	Seizure onset	3 yrs	50 days	2 mos	2 yrs	3 yrs	-	2 yrs	3 yrs
Motor findings	**Spasticity**	+	+	+	-	-	-	+	+
	Jitteriness/clonus	-	-	-	-	+	-	-	-
	Hypertonia	-	+	+	+	-	-	+	+
	Hypotonia	+	-	-	-	+ (Severe)	+ (Severe)	-	-
	Deep tendon reflexes	Increased	Increased	Increased	Increased	Decreased	Decreased	Increased	Increased
Visual findings	**Central visual impairment**	-	N/A	N/A	-	-	-	N/A	+
	Primary optic atrophy	-	N/A	N/A	-	-	-	N/A	+
	Nystagmus	-	N/A	N/A	-	-	-	N/A	-
	Strabismus	-	N/A	N/A	-	-	-	N/A	+
	Fixation and following	+	N/A	N/A	-	+/−	+/−	N/A	+
Developmental milestones (normal/delayed/absent)	**Gross motor**	Delayed/Absent	Delayed/Absent	Delayed/Absent	Delayed	Delayed/Absent	Delayed/Absent	Delayed	Delayed
	Fine motor	Absent	Absent	Absent	Delayed	Absent	Absent	Delayed	Delayed
	Language	Absent	Absent	Absent	Delayed	Delayed	Delayed	Absent	Absent
	Cognitive	Absent	Delayed/Absent	Absent	Delayed	Delayed/Absent	Delayed/Absent	Delayed	Delayed

		1810-VI-1	1327-IV-3 (died at 4 yo)	1327-IV-4	1327-IV-5	72597-II-1	72597-II-2	1337-II-1	1337-II-4
	Social	Delayed	Delayed	Delayed	Delayed	Delayed	Delayed	Delayed	Delayed
Diagnostic tests	**EMG**	7mos: Unremarkable 14 yrs: Muscle fibrillations	-	-	-	1 yr: Limited study unremarkable	-	-	-
	EEG	Severe slow waves of high amplitude	Left temporal discharges	N/A	N/A	Normal	Normal	Normal	Normal
MRI findings	**Cerebellum**	Atrophy	N/A	N/A	Atrophy	Atrophy	Atrophy	Atrophy	Atrophy
	Pons	Hypoplasia	N/A	N/A	Hypoplastic	Normal	Hypoplastic	Hypoplastic	Hypoplastic
	Cerebral cortex	Atrophy	N/A	N/A	Atrophy	Atrophy	Atrophy	Atrophy	Atrophy
	Ventricles	Enlarged	N/A	N/A	Enlarged	Normal	Normal	Enlarged	Enlarged
	White matter	Increased signal	N/A	N/A	Increased signal	Increased signal	Increased signal	Normal	Normal
	Corpus Callosum	Thin	N/A	N/A	Thin	Thin	Thin	Thin	Thin

HC: head circumference; EEG: electroencephalogram; EMG: electromyogram; SD: standard deviation below the mean. Progressive microcephaly noted by age-dependent decline in head circumference (SD, compare SD at birth to last exam). Electromyograph was normal in young patients (<1yr), but showed muscle fibrillations with increased patient age, indicative of motor neuron degeneration in patient 1810-VI-1. Additional clinical data found in Table S1.